

Cite this: *Dalton Trans.*, 2015, **44**, 18632

Different topologies in three manganese- μ -azido 1D compounds: magnetic behavior and DFT-quantum Monte Carlo calculations†

Franz A. Mautner,^a Christian Berger,^a Michael Scherzer,^a Roland C. Fischer,^b Lindley Maxwell,^c Eliseo Ruiz^c and Ramon Vicente^{*d}

The syntheses and structural characterization of three new monodimensional azido-bridged manganese(II) complexes with empirical formulae $[\text{Mn}(\text{N}_3)_2(\text{aminopyz})_2]_n$ (**1**), $[\text{Mn}(\text{N}_3)_2(4\text{-azpy})_2]_n$ (**2**) and $[\text{Mn}(\text{N}_3)_2(4\text{-Bzpy})_2]_n$ (**3**) (pyz = pyrazine (1,4-diazine)), 4-azpy = 4-azidopyridine and 4-Bzpy = 4-benzoylpyridine) are reported. **1** is a monodimensional compound with double EO azido bridges, **2** is an alternating monodimensional compound with double end-on and double end-to-end azido bridges in the sequence di-EO-di-EE and **3** is a monodimensional compound with double end-on and double end-to-end azido bridges in the sequence di-EO-di-EO-di-EO-di-EO-di-EE. The magnetic properties of **1–3** are reported. Periodic DFT calculations were performed to estimate the J values and quantum Monte Carlo simulations were carried out using the calculated J values to check their accuracy in comparison with the experimental magnetic measurements. From this theoretical analysis, two appealing features of the di-EO Mn(II) compounds can be extracted: first, the exchange coupling becomes more ferromagnetic when the Mn–N–Mn bridging angle becomes larger and the spin density of the bridging nitrogen atoms has an opposite sign to that of the Mn(II) centers.

Received 7th August 2015,
Accepted 21st September 2015

DOI: 10.1039/c5dt03034j

www.rsc.org/dalton

Introduction

In the last few years a plethora of polynuclear Mn(II)-azido bridging compounds have been prepared with the aim to expand the borders of the molecular magnetism field. One of the usual synthetic strategies mixes the $S = 5/2$ Mn(II) cation with the potentially bridging azido ligand and a terminal L ligand to obtain a large number of compounds with the general formula $[\text{Mn}(\text{N}_3)_2(\text{L})_2]$. L are usually R-pyridine monodentate ligands or $(\text{L})_2$ a bidentate aromatic N-donor ligand.

These $[\text{Mn}(\text{N}_3)_2(\text{L})_2]$ compounds show the entire range of dimensionalities: from molecular to 3D systems.^{1–13} Furthermore, the azido bridging ligand can show several coordination modes as the $\mu_{1,3}$ (end-to-end, EE) or $\mu_{1,1}$ (end-on, EO) modes, which can be present simultaneously in the same compound, generating a great variety of topologies in 1D–3D compounds. Taking into account that the EE coordination mode typically promotes antiferromagnetic, AF, interactions and the EO coordination mode promotes ferromagnetic, F, interactions, the great diversity of dimensionalities and topologies found in the Mn(II)-azido bridging compounds has as a consequence a great diversity in their magnetic behaviour: for example, in the 1D compound with the bulk formula $[\text{Mn}(\text{N}_3)_2(3\text{-Mepy})_2]_n$ (3-Mepy = 3-methylpyridine) the sequence of the azido bridges is $(\text{EE-EE-EO})_n$ which implies an $(\text{AF-AF-F})_n$ interaction pattern and a ferrimagnetic behaviour in a homometallic chain.¹⁴ This topological ferrimagnetism is found also in the 2D compound $[\text{Mn}(4\text{-N}_3\text{py})_2(\text{N}_3)_2]_n$ (4-N₃py = 4-azidopyridine) with the same (EE-EE-EO) alternance pattern in two dimensions.^{15a} As a consequence of their rich magnetic and structural variety, the polynuclear Mn(II)-azido bridging compounds have also been extensively used in magneto-structural correlations and theoretical studies.¹ We present in this work three monodimensional compounds which are new good examples of the wide

^aInstitut für Physikalische and Theoretische Chemie, Technische Universität Graz, Stremayrgasse 9, A-8010 Graz, Austria

^bInstitut für Anorganische Chemie, Technische Universität Graz, Stremayrgasse 9, A-8010 Graz, Austria

^cDepartament de Química Inorgànica and Institut de Química Teòrica i Computacional (IQTIC), Diagonal 645, 08028 Barcelona, Spain

^dDepartament de Química Inorgànica and Institut de Nanociència i Nanotecnologia de la Universitat de Barcelona (IN²UB), Martí i Franqués 1-11, 08028 Barcelona, Spain. E-mail: ramon.vicente@qi.ub.es; Fax: +34 93490 7725

† Electronic supplementary information (ESI) available: Table S1. Reported Mn(II) end-on azido compounds (labeled with the CSD REFCODE) showing the Mn–N–Mn bond angles (in degrees) and the experimental exchange coupling constants J (cm^{-1}) for such compounds. CCDC 1411985–1411987 (1–3). For ESI and crystallographic data in CIF or other electronic format see DOI: 10.1039/c5dt03034j



structural and magnetic diversity found in the $[\text{Mn}(\text{N}_3)_2(\text{L})_2]$ compounds: $[\text{Mn}(\text{N}_3)_2(\text{aminopyz})_2]_n$ (**1**), $[\text{Mn}(\text{N}_3)_2(4\text{-azpy})_2]_n$ (**2**) and $[\text{Mn}(\text{N}_3)_2(4\text{-Bzpy})_2]_n$ (**3**) (pyz = pyrazine (1,4-diazine)), 4-azpy = 4-azidopyridine and 4-Bzpy = 4-benzoylpyridine. **1** is a monodimensional compound with double EO azido bridges, **2** is an alternating monodimensional compound with double end-on and double end-to-end azido bridges in the sequence di-EO-di-EE and **3** is a monodimensional compound with double end-on and double end-to-end azido bridges in the sequence di-EO-di-EO-diEO-di-EO-di-EE. A preliminary crystal structure of **2** was published recently^{15b} but for this work we have obtained new crystals of the compound and the quality of X-ray data is improved. The magnetic properties of **1–3** are reported. The plot of χ_{MT} vs. T for **1** can be fitted as a homogeneous 1D system with $J = 1.4(1) \text{ cm}^{-1}$ and the plot of χ_{MT} vs. T for **2** can be fitted as an alternating F–AF 1D system with $J_1 = -12.8(1) \text{ cm}^{-1}$ and $J_2 = 0.7(1) \text{ cm}^{-1}$. The exchange coupling constants J have also been calculated for **1–3** by using periodic DFT calculations. In order to check the accuracy of the calculated J values, Quantum Monte Carlo (QMC) simulations were performed to extract susceptibility curves that can be compared with the experimental ones. In general, such a theoretical approach combining periodic calculations and QMC simulations is an accurate procedure to study the exchange interactions in extended structures due to the limitations of the fitting procedures of the experimental data.

Experimental section

Starting materials

Manganese(II) salts, organic N-donor ligands and sodium azide (Aldrich) were used as obtained. Aqueous hydrazoic acid is obtained with a modified Kipp's generator by decomposition of NaN_3 in $\text{H}_2\text{SO}_4/\text{H}_2\text{O}$ (1 : 3, v : v) and subsequent transfer of HN_3 into H_2O with the aid of an inert gas stream.¹⁶ The use of diluted hydrazoic acid allows the formation of an acidic medium with pH value < 5.5 without introducing a foreign salt, thus avoiding impurities. The synthesis of 4-azidopyridine was performed according to the literature.¹⁷

Caution! Azide compounds and hydrazoic acid (HN_3) are potentially explosive! Only a small amount of material should be prepared and it should be handled with care.

Spectral and magnetic measurements

Infrared spectra ($4000\text{--}400 \text{ cm}^{-1}$) were recorded from KBr pellets on a Perkin-Elmer 380-B spectrophotometer. Magnetic susceptibility measurements under several magnetic fields in the temperature range of 2–300 K and magnetization measurements in the field range of 0–5 T were performed with a Quantum Design MPMS-XL SQUID magnetometer at the Magnetic Measurements Unit of the University of Barcelona. All measurements were performed on polycrystalline samples. Pascal's constants were used to estimate the diamagnetic corrections, which were subtracted from the experi-

mental susceptibilities to give the corrected molar magnetic susceptibilities.

Synthesis

$[\text{Mn}(\text{N}_3)_2(\text{ampyz})_2]_n$ (**1**). Manganese(II) nitrate tetrahydrate (0.50 g, 2.0 mmol), sodium azide (0.26 g, 4.0 mmol) and aminopyrazine (0.19 g, 2.0 mmol) were dissolved in 3.5 mL aqueous hydrazoic acid. A clear solution was obtained after warming to 60 °C. Slow cooling of the solution to 4 °C gave after several days compound **1** as yellow crystals. Yield: 70%. Anal.: Found: C 29.0; H 3.0; N 51.3%. Calcd for $\text{C}_8\text{H}_{10}\text{MnN}_{12}$: C 29.2; H 3.1; N 51.1%.

$[\text{Mn}(\text{N}_3)_2(4\text{-azpy})_2]_n$ (**2**). Manganese(II) chloride dihydrate (0.161 g, 1.0 mmol) and 4-azidopyridine (0.240 g, 2.0 mmol) were added to 10.0 mL dist. H_2O . NaN_3 aqueous solution (1 M, 5 mL) was then slowly added with stirring. The solution was then put into a compartment dryer (50 °C) for four days. Afterwards the solution was stored at room temperature. Yellow crystals of **2** were obtained after some days. Yield: 84%. Anal.: Found: C 31.7; H 2.4; N 51.5%. Calcd for $\text{C}_{10}\text{H}_8\text{MnN}_{14}$: C 31.7; H 2.1; N 51.7%.

$[\text{Mn}(\text{N}_3)_2(4\text{-Bzpy})_2]_n$ (**3**). To an aqueous solution (4 mL) of manganese(II) nitrate tetrahydrate (0.50 g, 2.0 mmol) and sodium azide (0.26 g, 4.0 mmol) 20 mL of methanolic solution of 4-benzoylpyridine (0.37 g, 2.0 mmol) were added. The mixture was warmed to 60 °C to obtain a clear solution and subsequently allowed to stand in an open beaker at room temperature. After two weeks yellow needle-shaped crystals of compound **3** were separated. Yield: 60%. Anal.: Found: C 56.9; H 3.5; N 22.4%. Calcd for $\text{C}_{24}\text{H}_{18}\text{MnN}_8\text{O}_2$: C 57.0; H 3.6; N 22.2%.

IR spectra

In addition to the vibrations of the aromatic N-donor ligands, very strong absorption bands corresponding to the ν_{as} of the azido ligands appeared at 2100 cm^{-1} for **1**, at 2093 and 2054 cm^{-1} for **2**, and at 2105 and 2059 cm^{-1} for **3**.

X-ray crystallography

The X-ray single-crystal data of compounds **1–3** were collected on a Bruker SMART APEX CCD diffractometer with graphite-monochromated $\text{Mo K}\alpha$ radiation ($\lambda = 0.71073 \text{ \AA}$). The crystallographic data, the conditions retained for the intensity data collection and some features of the structure refinements are listed in Table 1. Data processing, Lorentz-polarization and absorption corrections were performed using SMART, APEX, SAINT, and SADABS¹⁸ computer programs. The structures were solved by direct methods and refined by full-matrix least-squares methods, using the SHELXTL program package.¹⁹ All non-hydrogen atoms were refined anisotropically. The hydrogen atoms were located from difference Fourier maps, assigned with isotropic displacement parameters and included in the refinements by the use of HFIX (parent C atoms) or DFIX (parent N atoms) utilities of the SHELXTL program package. Molecular plots were performed using the Mercury²⁰ program.



Table 1 Crystal data and structure refinement for complexes 1–3

Compound	1	2	3
Empirical formula	C ₈ H ₁₀ MnN ₁₂	C ₁₀ H ₈ MnN ₁₄	C ₁₂₀ H ₉₀ Mn ₅ N ₄₀ O ₁₀
Formula weight	329.22	379.24	2527.03
Crystal system	Triclinic	Triclinic	Monoclinic
Space group	<i>P</i> $\bar{1}$	<i>P</i> $\bar{1}$	<i>C</i> 2/ <i>c</i>
<i>a</i> (Å)	3.4751(5)	8.2450(3)	37.0077(13)
<i>b</i> (Å)	7.7427(7)	8.3050(3)	19.0045(7)
<i>c</i> (Å)	12.4280(14)	11.9444(5)	17.0615(6)
α (°)	101.48(2)	82.612(2)	90
β (°)	96.04(2)	69.905(2)	112.212(2)
γ (°)	96.73(2)	80.754(2)	90
<i>V</i> (Å ³)	322.60(7)	755.74(5)	11 109.1(7)
<i>Z</i>	1	2	4
<i>T</i> (K)	100(2)	100(2)	100(2)
ρ_{calcd} (g m ⁻³)	1.695	1.667	1.511
μ (mm ⁻¹)	1.040	0.904	0.635
Crystal size (mm)	0.35 × 0.18 × 0.08	0.38 × 0.22 × 0.17	0.48 × 0.14 × 0.11
θ_{max} (°)	26.35	31.70	25.30
Reflections collected	2589	23 052	62 737
<i>R</i> (int)	0.0219	0.0274	0.0523
Data	1298	4813	10 123
Parameters	107	226	791
<i>R</i> ^a [<i>I</i> > 2 σ (<i>I</i>)]	0.0452	0.0291	0.0455
<i>R</i> ² ω^b (all data)	0.1107	0.0688	0.1656

$$^a R(F_o) = \sum ||F_o| - |F_c|| / \sum |F_o|. \quad ^b R\omega(F_o)^2 = \{ \sum [\omega((F_o)^2 - (F_c)^2)] / \sum [\omega((F_o)^4)] \}^{1/2}.$$

Computational methods

The computer code employed for all the calculations is the program SIESTA^{21–23} (Spanish Initiative for Electronic Simulations with Thousands of Atoms) that allows handling periodic systems like those reported in this study. We have employed the generalized-gradient functional proposed by Perdew, Burke and Ernzerhof²⁴ using the DFT+*U* option²⁵ with a *U* value of 4.0 eV. Only valence electrons are included in the calculations, with the core being replaced by norm-conserving scalar relativistic pseudopotentials factorized in the Kleinman–Bylander form.²⁶ The pseudopotentials are generated according to the procedure of Trouiller and Martins.²⁷ For the Mn atoms we have employed a pseudopotential including the 3s and 3p orbitals in the basis set that we have previously tested to give accurate *J* values.²⁸ We have also employed a numerical basis set of triple- ζ quality with polarization functions for the manganese atoms and a double- ζ one with polarization functions for the main group elements. Previously, we have studied the influence of two main parameters of the SIESTA code, the energy shift and the mesh cut-off, in the calculated *J* value for transition metal systems.²⁹ Thus, the values of 50 meV for the energy shift and 250 Ry for the mesh cut-off provide a good compromise between accuracy and computer time to estimate exchange coupling constants. The calculated *J* values are obtained with the non-spin projected approach^{30–33} and using the following Heisenberg–Dirac–van Vleck Hamiltonian:

$$\hat{H}^{\text{HDVV}} = - \sum_{i>j} J_{ij} \hat{S}_i \hat{S}_j \quad (1)$$

A detailed description of how to calculate the *J* values of periodic systems was previously reported by some of us.³⁴ For compound **1**, two calculations were performed to extract the unique *J* value as the energy difference between the high spin solution (both metal atoms in the unit cell with spin up) and the low spin solution (with the spin inversion of one of the paramagnetic centers). For compounds **2** and **3**, three and six spin configurations were employed to calculate the *J* values. A supercell duplicating the length in the direction of the chain must be created to calculate the exchange constants; thus, for compounds **1**, **2** and **3** in the periodic calculations the system has 62, 132 and 1060 atoms, respectively. Sets of 462, 12 and 1 *k*-points were employed, respectively, for **1**, **2** and **3** to integrate the *k*-dependent properties.

The usual procedure to check the accuracy of the calculated *J* values is by the generation of the χT curves for comparison with the experimental data. The best procedure for obtaining such curves is to perform exact diagonalization of the Hamiltonian. However, such an approach cannot be applied for periodic systems and it is thus necessary to use approximate methods in order to make a comparison with the experimental data. Quantum Monte Carlo methods represent a good alternative. Quantum Monte Carlo simulations based on the directed loop algorithm method developed by Sandvik *et al.*³⁵ were performed using the ALPS 2.0 library (dirloop_sse package).^{36,37} For the susceptibility *vs.* temperature curve, usually we set 10⁷ steps for simulations between 2 and 300 K and a whole simulation must be performed at each temperature. The initial 10% of the steps was employed for thermalization of the system in all calculations. However, 10⁹ steps were employed below in



order to reach the convergence of the simulations using the DFT calculated J values.

Results and discussion

Description of the structures

Description of the structure of $[\text{Mn}(\text{N}_3)_2(\text{aminopyrazine})_2]_n$ (1). Compound 1 crystallizes in the triclinic space group $P\bar{1}$. Relevant bond lengths and bond angles are listed in Table 2. Fig. 1a illustrates the structure. Each Mn is coordinated by six N atoms in octahedral geometry. Four coordination sites are occupied by azido groups which double-bridge the Mn atoms in end-on only coordination mode to give 1-D chains along the a -axis of the unit cell [$\text{Mn}\cdots\text{Mn} = 3.4751(5)$ Å]. The octahedron is completed by two *trans* coordinated N atoms provided by two aminopyrazine ligands bonded *via* the aromatic nitrogen in the *meta* position to the amino sidegroup. Mn(1) and the center of the Mn(1)–N(11)–Mn(1b)–N(11b) rhomboid are located at centers of inversions. The azido group is out of the Mn_2N_2 plane with an angle of $159.5(2)^\circ$ for N(11b) \cdots N(11)–N(12). Both hydrogen atoms of the $-\text{NH}_2$ group establish hydrogen bonds to N atoms in adjacent chains giving rise to a 2-D supramolecular network (Fig. 1b). Hydrogen acceptors are the terminal N atom of the azido groups and the non-coordinated aromatic N atom of the aminopyrazine ligands. Along the chain direction the pyrazine rings form π – π stacking interactions.

Description of the structure of $[\text{Mn}(\text{N}_3)_2(4\text{-azpy})_2]_n$ (2). The atom numbering scheme for complex 2 is given in Fig. 2a, and selected bond parameters are given in Table 3. The structure consists of octahedrally coordinated manganese atoms in which the coordination sites are occupied by two N atoms of the 4-azidopyridine ligands in *trans* arrangement and four azido ligands from double bridges between neighboring manganese atoms. The Mn–N bond lengths are in the range from 2.2156(11) to 2.2701(12) Å. The azido groups in the double bridges are alternatively in the EE and EO modes generating an alternating chain oriented along the b -axis of the

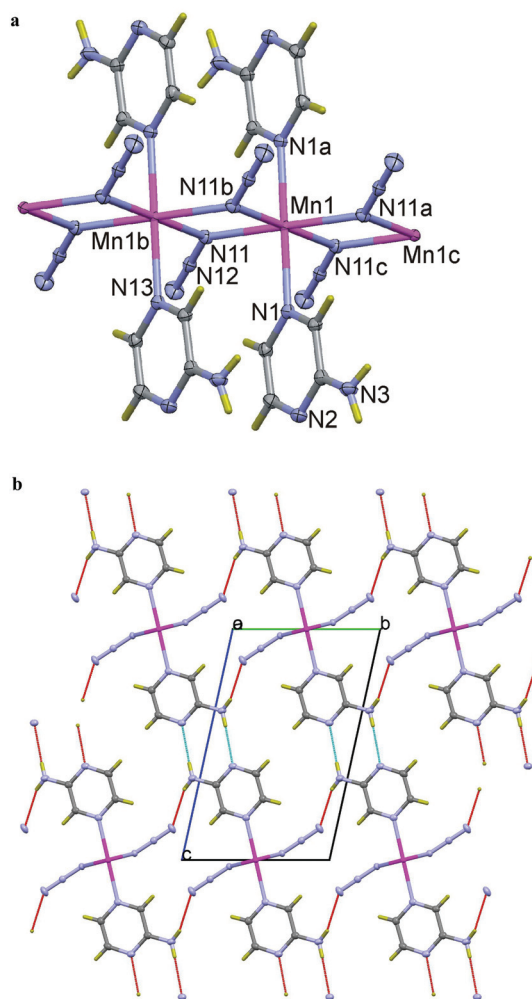


Fig. 1 (a) Perspective view of 1 showing the atom-numbering scheme. Symmetry codes: (a) $-x + 1, -y + 1, -z$; (b) $-x + 2, -y + 1, -z$; (c) $x + 1, y, z$. (b) Packing view of 1. Broken bonds indicate hydrogen bonds.

Table 2 Selected bond lengths (Å) and angles ($^\circ$) for (1)

Mn(1) \cdots Mn(1b)	3.4751(5)	Mn(1)–N(11a)	2.232(2)
Mn(1)–N(11c)	2.250(2)	Mn(1)–N(1a)	2.272(2)
N(11)–N(12)	1.212(3)	N(12)–N(13)	1.148(3)
N(3)–H(5)	0.79	H(5) \cdots N(13d)	2.36
N(3) \cdots N(13d)	3.121(4)	N(3)–H(6)	0.84
H(6) \cdots N(2e)	2.20	N(3) \cdots N(2e)	3.037(3)
N(11a)–Mn(1)–N(11)	180.0	N(11a)–Mn(1)–N(11b)	101.53(5)
N(11)–Mn(1)–N(11b)	78.47(5)	N(11b)–Mn(1)–N(11c)	180.0
N(11a)–Mn(1)–N(1a)	91.07(9)	N(11c)–Mn(1)–N(1a)	92.58(9)
N(11b)–Mn(1)–N(1a)	87.42(9)	N(11a)–Mn(1)–N(1)	88.93(9)
N(1a)–Mn(1)–N(1)	180.0	N(12)–N(11)–Mn(1)	132.26(19)
N(12)–N(11)–Mn(1b)	120.74(19)	Mn(1)–N(11)–Mn(1b)	101.67(9)
N(13)–N(12)–N(11)	179.4(3)	N(11b) \cdots N(11)–N(12)	159.5(2)
N(3)–H(5) \cdots N(13d)	162	N(3)–H(6) \cdots N(2e)	174

Symmetry codes: (a) $-x + 1, -y + 1, -z$; (b) $-x + 2, -y + 1, -z$; (c) $x - 1, y, z$; (d) $x - 1, y + 1, z$; (e) $-x + 1, -y + 2, -z + 1$.

triclinic unit cell (Fig. 2b). The end-on azido bridges show asymmetric N–N distances of 1.2041(16)/1.1497(17) Å, whereas the end-to-end bridges are more symmetric: 1.1794(15)/1.1754(15) Å. The bond parameters within the $\text{Mn}_2(\mu_{1,3}\text{-N}_3)_2$ ring are: N(4)–Mn(1)–N(5) = $99.31(4)^\circ$, Mn(1)–N(5)–N(6) = $123.85(10)^\circ$, Mn(1)–N(4)–N(6b) = $119.91(9)^\circ$, torsion angle: Mn(1b)–N(5b) \cdots N(4)–Mn(1) = 50.9° . This eight-membered ring $\text{Mn}_2(\mu_{1,3}\text{-N}_3)_2$ shows a distortion from the planar to a “chair”-like conformation with a δ -angle [defined as the dihedral angle between the plane defined for the six N-azido atoms and the N(4)–Mn(1)–N(5) plane] of 34.0° , whereas the four-membered $\text{Mn}_2(\mu_{1,1}\text{-N}_3)_2$ ring is planar. The intra-chain Mn \cdots Mn distance within the four-membered ring is 3.6344(3) Å, and that within the eight-membered ring is 5.0301(3) Å, whereas the shortest inter-chain metal \cdots metal separation is 8.2450(5) Å. The bond parameters of the di-EO azido bridge are: N(1)–Mn(1)–N(1a) = $81.25(5)^\circ$, Mn(1)–N(1a)–Mn(1a) = $98.75(5)^\circ$, Mn(1)–N(1)–N(2) = $126.07(9)^\circ$, Mn(1a)–N(1)–N(2) = $126.32(9)^\circ$, N(1a) \cdots N(1)–N(2) “out-of plane angle” = $155.1(2)^\circ$. The azido ligands have



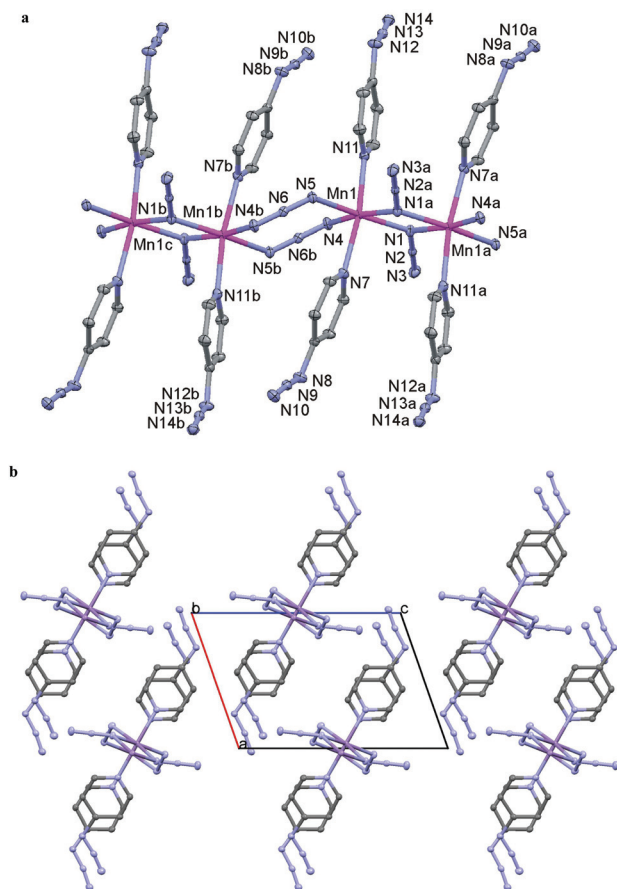


Fig. 2 (a) A section of the chain structure of **2** showing the atom numbering scheme. Symmetry codes: (a) $-x + 2, -y, -z$; (b) $-x + 1, -y, -z$; (c) $x + 1, y, z$. (b) Packing view of **2**.

Table 3 Selected bond lengths (Å) and angles (°) for (**2**)

Mn(1a)–N(1)	2.2156(11)	Mn(1)–N(1)	2.2172(11)
Mn(1)–N(11)	2.2369(12)	Mn(1)–N(4)	2.2400(12)
Mn(1)–N(5)	2.2450(12)	Mn(1)–N(7)	2.2701(12)
N(1)–N(2)	1.2041(16)	N(2)–N(3)	1.1497(17)
N(5)–N(6)	1.1754(15)	N(6)–N(4b)	1.1794(15)
N(4b)–N(6)	1.1795(15)	N(11)–C(6)	1.3384(18)
N(11)–C(10)	1.3403(18)	N(12)–N(13)	1.2536(17)
N(12)–C(8)	1.4113(18)	N(13)–N(14)	1.1181(17)
N(7)–C(5)	1.3379(18)	N(7)–C(1)	1.3411(17)
N(8)–N(9)	1.2465(17)	N(8)–C(3)	1.4139(18)
N(9)–N(10)	1.1243(17)		
N(1a)–Mn(1)–N(1)	81.25(5)	N(1a)–Mn(1)–N(11)	94.13(4)
N(1)–Mn(1)–N(11)	93.82(4)	N(1a)–Mn(1)–N(4)	170.27(4)
N(1)–Mn(1)–N(4)	89.33(4)	N(11)–Mn(1)–N(4)	88.93(4)
N(1a)–Mn(1)–N(5)	90.09(4)	N(1)–Mn(1)–N(5)	171.34(4)
N(11)–Mn(1)–N(5)	86.79(4)	N(4)–Mn(1)–N(5)	99.31(4)
N(1a)–Mn(1)–N(7)	91.85(4)	N(1)–Mn(1)–N(7)	93.60(4)
N(11)–Mn(1)–N(7)	171.10(4)	N(4)–Mn(1)–N(7)	86.25(4)
N(5)–Mn(1)–N(7)	86.62(4)	N(2)–N(1)–Mn(1a)	126.32(9)
N(2)–N(1)–Mn(1)	126.07(9)	Mn(1a)–N(1)–Mn(1)	98.75(5)
N(3)–N(2)–N(1)	179.48(14)	N(6)–N(5)–Mn(1)	123.85(10)
N(5)–N(6)–N(4b)	178.74(14)	N(6)–N(4)–Mn(1b)	119.91(9)
C(6)–N(11)–C(10)	116.87(12)	C(6)–N(11)–Mn(1)	120.85(9)
C(10)–N(11)–Mn(1)	122.28(10)	N(13)–N(12)–C(8)	116.50(12)
N(14)–N(13)–N(12)	170.95(15)		

Symmetry codes: (a) $-x, 1 - y, 1 - z$; (b) $-x, -y, 1 - z$.

N–N–N bond angles of $179.48(14)^\circ$ and $178.74(14)^\circ$, respectively. The two axially bound 4-azidopyridine ligands show an angle of N(11)–Mn(1)–N(7) of $171.10(4)^\circ$. The reason for this deviation from 180° is due to the moving of the axial ligands away from the Mn_2N_2 ring. The covalent azido groups in the *para*-position (from 4-azidopyridine) are highly asymmetric, with $\Delta d(\text{N–N})$ (difference of N–N bond lengths within the azido group) of $0.1355(18)$ Å and $0.1222(18)$ Å. The according bond angle for N(14)–N(13)–N(12) is $170.95(15)^\circ$ and for N(10)–N(9)–N(8) is $171.14(15)^\circ$.

Description of the structure of $[\text{Mn}(\text{N}_3)_2(4\text{-Bzpy})_2]_n$ (3**).** A perspective view of a section of the neutral polymeric $[\text{Mn}(4\text{-Bzpy})_2(\text{N}_3)_2]_n$ chain of **3** together with the atom numbering scheme is given in Fig. 3a, and selected bond parameters are given in Table 4. The Mn(II) centers are octahedrally coordinated by two N donor atoms of the 4-Bzpy ligands in *trans*-arrangement and four N atoms of azido bridges. The Mn–N (N_3) bond distances are in the range from $2.221(4)$ to $2.248(4)$ Å, and the Mn–N(4-Bzpy) bond distances vary from $2.283(3)$ to $2.293(3)$ Å. The azido bridges show an alternating Mn(5)–(EO)₂–Mn(2)–(EO)₂–Mn(1)–(EO)₂–Mn(3)–(EO)₂–Mn(4)–(EE)₂–sequence giving rise to the 1D system, which is oriented along the *b*-axis of the monoclinic unit cell (Fig. 3b). The Mn(4)–(EE)₂–Mn(5b) azido bridge has an almost planar arrangement with a δ -angle of 3.6° . The Mn(4)⋯Mn(5b) intra-chain distance is $5.1413(13)$ Å, and the Mn(4)–N(51)⋯N(53b)–Mn(1b) torsion angle is -15.9° . The four-membered Mn_2N_2 rings formed by the four consecutive di-EO azido bridges have intra-chain metal⋯metal distances of $3.4693(12)$, $3.4735(12)$, $3.4634(12)$ and $3.4571(12)$ Å; and the Mn–N–Mn bond angles are in the range from $101.14(15)$ to $101.42(15)^\circ$. The angles N(X1a)⋯N(X1)–N(X2) ($X = 1-4$) are $175.0(4)$, $172.9(4)$, $176.1(4)$ and $174.1(4)^\circ$, respectively. The azido bridges have Mn–N–N and N–N–N bond angles varying from $123.6(3)$ to $135.3(3)$ and from $177.7(5)$ to $179.5(4)^\circ$, respectively. The *trans*-pyridine rings of the 4-Bzpy ligands are shifted towards the di-EE azido bridges [N(py)–Mn–N(py) bond angles: $178.24(18)^\circ$ for Mn(1), $177.40(17)^\circ$ for Mn(2), $174.02(16)^\circ$ for Mn(3), $165.18(19)^\circ$ for Mn(4) and $168.60(19)^\circ$ for Mn(5), respectively]. Non-covalent ring–ring interactions are observed along the chain direction with separation of their centers of gravities in the range from 3.635 to 4.287 Å for the pyridine rings and in the range from 3.770 to 3.870 Å for the benzene rings of the 4-Bzpy ligands, respectively.

Magnetic data for $[\text{Mn}(\text{N}_3)_2(\text{aminopyrazine})_2]_n$ (1**).** The variable temperature magnetic susceptibility data for the title complex were recorded between 300 and 2 K. The plot of $\chi_{\text{M}}T$ versus T is shown in Fig. 4. Compound **1** shows a $\chi_{\text{M}}T$ value of 4.85 cm³ mol⁻¹ K at room temperature, greater than the expected value for an isolated manganese atom (4.375 cm³ mol⁻¹ K, $g = 2.0$), and increases gradually as the temperature decreases to a maximum of 17.25 cm³ mol⁻¹ K at 5 K and then decreases quickly to 8.15 cm³ mol⁻¹ K at 2 K. The magnetic susceptibility behaviour of **1** indicates bulk ferromagnetic coupling in good agreement with magnetization experiments which show a quasi-saturated value of



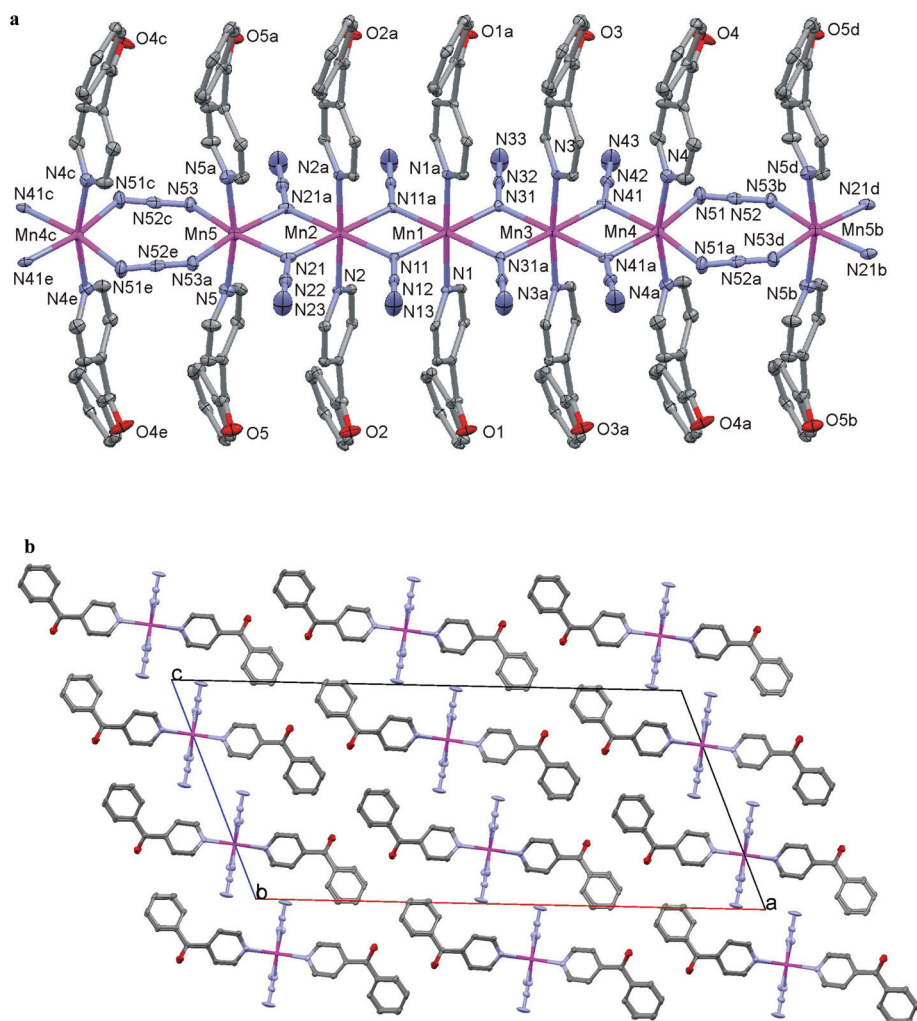


Fig. 3 (a) A section of the 1-D system of **3** showing the atom-numbering scheme. Symmetry codes: (a) $-x, y, 1/2 - z$; (b) $x, 1 + y, z$; (c) $x, -1 + y, z$; (d) $-x, 1 + y, 1/2 - z$; (e) $-x, -1 + y, 1/2 - z$. (b) Packing view of **3**.

$M/N\beta$ equivalent to five electrons (5.13) under an external field of 5 T at 2 K. Taking into account the 1D structure of **1**, the fit of the magnetic data was done by using the appropriate equation³⁸ for homogeneous $S = 5/2$ chains derived from the Hamiltonian $H = -JS_i S_{i+1}$ in the range 300–8 K due to the decrease of the $\chi_M T$ values after the maximum. The best fit parameters were $J = 1.4(1) \text{ cm}^{-1}$, $g = 2.09(1)$. The positive J value is in accordance with the ferromagnetic coupling expected for end-on azido bridges with Mn–N–Mn bond angles of around 100° (the Mn(1)–N(11)–Mn(1') bond angle is $101.53(5)^\circ$). The found J value is similar to that reported for the related compounds *cis*-[Mn($\mu_{1,1}$ -N₃)₂(2-bzpy)₂]_n (2-bzpy = 2-benzoylpyridine)³⁹ and *trans*-[Mn($\mu_{1,1}$ -N₃)₂(pyzamid)₂]_n (pyzamid = pyrazineamide)⁴⁰ with J values of 0.8 and 1.1 cm^{-1} for Mn–N–Mn angles of 100.5° (mean angle) and 97.1° respectively. The structure of *cis*-[Mn($\mu_{1,1}$ -N₃)₂(2-bzpy)₂]_n shows well isolated chains but as in the case of *trans*-[Mn($\mu_{1,1}$ -N₃)₂(pyzamid)₂]_n, **1** shows H bonds between chains which can be the cause of the weak antiferromagnetic interactions at low

temperature as can be seen from the decrease of $\chi_M T$ in the low temperature region.

Magnetic data for [Mn(N₃)₂(4-azpy)₂]_n (2**).** The variable temperature magnetic susceptibility data for the title complex were recorded between 300 and 2 K. The plot of $\chi_M T$ versus T is shown in Fig. 5. Compound **2** shows a $\chi_M T$ value of $3.83 \text{ cm}^3 \text{ mol}^{-1} \text{ K}$ at room temperature, lesser than the expected value for an isolated manganese atom ($4.375 \text{ cm}^3 \text{ mol}^{-1} \text{ K}$, $g = 2.0$), and decreases gradually as the temperature decreases to a minimum of $0.02 \text{ cm}^3 \text{ mol}^{-1} \text{ K}$ at 2 K. The magnetic susceptibility behaviour of **2** indicates bulk antiferromagnetic coupling in good agreement with magnetization experiments which show a quasi-saturated value of $M/N\beta$ equivalent to zero electrons (0.06) under an external field of 5 T at 2 K. Taking into account the alternating 1D structure of **2**, the fit of the magnetic data was done by using the appropriate equation⁴¹ for ferromagnetic–antiferromagnetic coupled 1D $S = 5/2$ systems derived from the Hamiltonian $H = -J_1 \sum S_{2i} S_{2i+1} - J_2 \sum S_{2i+1} S_{2i+2}$. The best fit parameters were $J_1 = -12.8(1) \text{ cm}^{-1}$, $J_2 = 0.7(1)$



Table 4 Selected bond lengths (Å) and angles (°) for (3)

Mn(1)–N(11)	2.243(4)	Mn(2)–N(11)	2.240(4)
Mn(1)–N(31)	2.248(4)	Mn(2)–N(21)	2.240(4)
Mn(1)–N(1)	2.289(3)	Mn(2)–N(2)	2.293(3)
Mn(3)–N(31)	2.242(4)	Mn(4)–N(41)	2.239(4)
Mn(3)–N(41)	2.236(4)	Mn(4)–N(51)	2.221(4)
Mn(3)–N(3)	2.291(3)	Mn(4)–N(4)	2.283(3)
Mn(5)–N(21)	2.236(4)	N(11)–N(12)	1.186(5)
Mn(5)–N(53)	2.221(4)	N(12)–N(13)	1.152(5)
Mn(5)–N(5)	2.287(4)	N(21)–N(22)	1.178(5)
N(22)–N(23)	1.156(6)	N(31)–N(32)	1.181(5)
N(32)–N(33)	1.153(6)	N(41)–N(42)	1.192(5)
N(42)–N(43)	1.144(6)	N(51)–N(52)	1.160(5)
N(52)–N(53b)	1.176(5)		
N(11)–Mn(1)–N(31)	179.34(13)	N(1)–Mn(1)–N(1a)	178.24(18)
N(11)–Mn(2)–N(21a)	179.74(12)	N(2)–Mn(2)–N(2a)	177.40(17)
N(41a)–Mn(3)–N(31)	178.65(13)	N(3)–Mn(3)–N(3a)	174.02(16)
N(41)–Mn(4)–N(51a)	168.48(15)	N(4)–Mn(4)–N(4a)	165.18(19)
N(21)–Mn(5)–N(53)	168.76(15)	N(5)–Mn(5)–N(5a)	168.60(19)
Mn(1)–N(11)–N(12)	130.4(3)	Mn(2)–N(11)–N(12)	127.8(3)
Mn(2)–N(21)–N(22)	134.4(3)	Mn(5)–N(21)–N(22)	123.9(3)
Mn(1)–N(31)–N(32)	130.7(3)	Mn(3)–N(31)–N(32)	127.7(3)
Mn(3)–N(41)–N(42)	135.3(3)	Mn(4)–N(41)–N(42)	123.6(3)
Mn(4)–N(51)–N(52)	127.4(3)	Mn(5)–N(53)–N(52c)	127.9(3)
Mn(1)–N(11)–Mn(2)	101.42(15)	Mn(2)–N(21)–Mn(5)	101.37(15)
Mn(1)–N(31)–Mn(3)	101.35(15)	Mn(3)–N(41)–Mn(4)	101.14(15)
N(11)–N(12)–N(13)	179.5(4)	N(21)–N(22)–N(23)	179.4(5)
N(31)–N(32)–N(33)	179.2(4)	N(41)–N(42)–N(43)	179.2(4)
N(51)–N(52)–N(53b)	177.7(5)		

Symmetry codes: (a) $-x, y, 1/2 - z$; (b) $x, 1 + y, z$; (c) $x, -1 + y, z$; (d) $-x, 1 + y, 1/2 - z$; (e) $-x, -1 + y, 1/2 - z$.

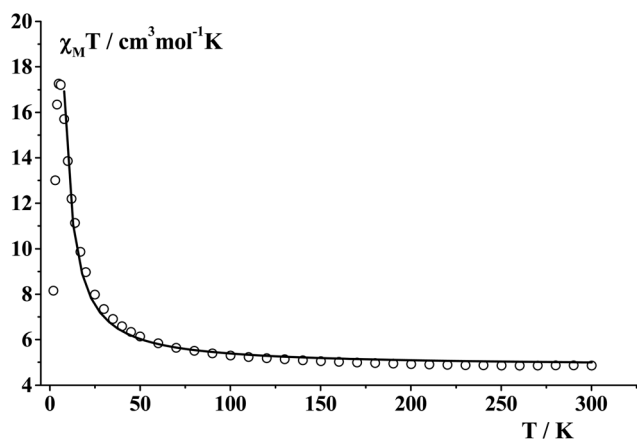


Fig. 4 $\chi_M T$ vs. T plot in the 300–2 K range of temperatures for 1. The solid line shows the best fit as a uniform chain (see the text).

cm^{-1} , $g = 2.06(1)$. The positive J value is in accordance with the ferromagnetic coupling expected for end-on azido bridges with Mn–N–Mn bond angles of around 100° (the Mn(1)–N(1a)–Mn(1a) bond angle is $98.75(5)^\circ$). The found J value is similar to that reported for the related compounds cis -[Mn($\mu_{1,1}$ -N₃)₂-(2-bzpy)₂]_n (2-bzpy = 2-benzoylpyridine)³⁹ and $trans$ -[Mn($\mu_{1,1}$ -N₃)₂-(pyzamid)₂]_n (pyzamid = pyrazineamide)⁴⁰ with J values of 0.8 and 1.1 cm^{-1} for Mn–N–Mn angles of 100.5° (mean angle) and 97.1° respectively.

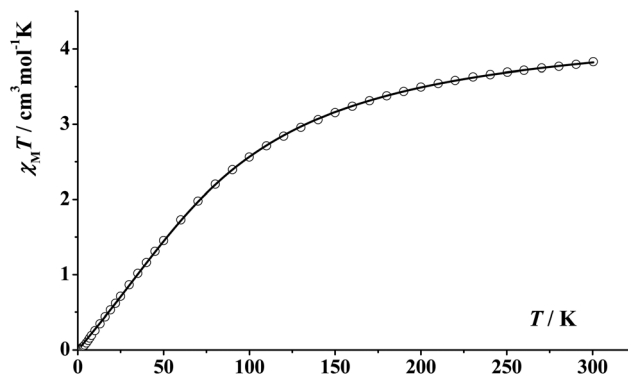


Fig. 5 $\chi_M T$ vs. T plot in the 300–2 K range of temperatures for 2. The solid line shows the best fit as an alternating chain (see the text).

Magnetic data for [Mn(N₃)₂(4-Bzpy)₂]_n (3). The plot of $\chi_M T$ versus T in the 300–2 K range of temperature for compound 3 is shown in Fig. 6. Compound 3 shows a $\chi_M T$ value of $4.31 \text{ cm}^3 \text{ mol}^{-1} \text{ K}$ at room temperature, similar to the expected value for an isolated manganese atom ($4.375 \text{ cm}^3 \text{ mol}^{-1} \text{ K}$, $g = 2.0$). On cooling, $\chi_M T$ decreases to $3.72 \text{ cm}^3 \text{ mol}^{-1} \text{ K}$ at 60 K. Below this broad minimum, $\chi_M T$ increases to a maximum of $3.87 \text{ cm}^3 \text{ mol}^{-1} \text{ K}$ at 20 K and then falls to $1.18 \text{ cm}^3 \text{ mol}^{-1} \text{ K}$ at 2 K. The magnetization measurements show a saturation value close to $S = 3/2$ per manganese ion (inset of Fig. 6). This value is striking as the ground state of this chain should be $S = 0$ (Scheme 1). The $\chi_M T$ decay observed below 20 K corresponds

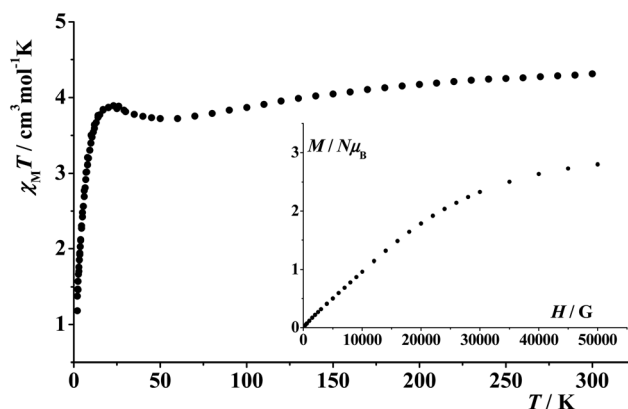
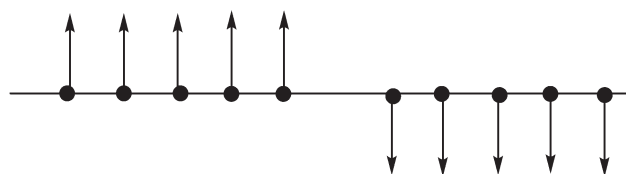


Fig. 6 $\chi_M T$ vs. T plot in the 300–2 K range of temperatures for 3. Inset: molar magnetization at 2 K for 3.



Scheme 1 Ground state for an $(AF-F-F-F-F-F)_n$ interaction sequence.



to the population of the ground state. Similar behaviour has been observed in the 1D compound¹⁴ *trans*-[Mn(N₃)₂(Menic)₂]_n showing the same topology as **3**.

Theoretical study. The structural dependence of the exchange coupling in end-on azido-bridged Mn(II) dinuclear complexes was previously studied by using hybrid DFT methods.⁴² Thus, it is expected that end-on coordination results in ferromagnetic behavior⁴³ while the opposite is found for end-to-end azido bridging ligands. The calculated values for the three studied systems are given in Table 5. It is worth noting that generalized gradient approximation functionals, such as PBE, are less accurate than hybrid functionals to calculate the *J* values.^{30–33} However, computer codes to calculate periodic systems usually have not implemented hybrid functionals in an efficient way; hence, we have employed the PBE functional that usually gives good results for transition metal complexes. The calculated *J* values show that the PBE functional reproduces properly the sign of the interaction; thus, exchange couplings through end-on azido ligands are ferromagnetic while those with end-to-end coordination are stronger and antiferromagnetic. In order to make a comparison with the experimental data, the calculated DFT *J* values (see Table 5) were employed along with quantum Monte Carlo simulations (see the Computational methods section) to calculate magnetic susceptibility curves that can be directly compared with the experimental data. Excellent agreement is found in Fig. 7 showing that the employed DFT methodology is able to reproduce the experimental magnetic properties of these systems.

Concerning the strength of the interaction, there is a “general belief” that the increase of the M–X–M angle for bridging ligands with a single atom in the exchange pathway enhances the antiferromagnetic contributions. As mentioned above, previously we performed a theoretical study using the B3LYP functional to analyze the dependence between *J* and the Mn–N–Mn bridging angle for dinuclear azido ligands, as well as for the equivalent systems with Cu(II) and Ni(II) cations. In the three cases, there is a parabolic dependence showing a maximum of the parabola that corresponds to the strongest ferromagnetic coupling.⁴² This maximum appears at M–N–M angle values of 85°, 102° and 112° for Cu(II), Ni(II) and Mn(II) complexes, respectively. Thus, as most of the Cu(II) complexes have a Cu–N–Cu angle larger than 85° the tendency is in agreement with the “expected” behavior, larger Cu–N–Cu increases the antiferromagnetic contribution and the complexes become less ferromagnetic. For the Ni(II) complexes, the maximum strength of the ferromagnetic interaction appears for Ni–N–Ni angle values close to those adopted in most of the structures.⁴⁴ Thus, most of the Ni(II) azido bridging complexes show a small dispersion in the *J* values being ferromagnetic, and only a reported complex with a Ni–N–Ni angle value close to 90° presents antiferromagnetic behavior.⁴⁵ However, the Mn(II) complexes adopt Mn–N–Mn angle values smaller than that corresponding to the strongest ferromagnetic coupling. Thus, an increase of the Mn–N–Mn angle value enhances the ferromagnetism and such a tendency is just the opposite of the one usually assumed. This fact can be corroborated in Fig. 8 showing the dependence of the fitted *J* value for the reported EO azido Mn(II) complexes with the Mn–N–Mn angle value.

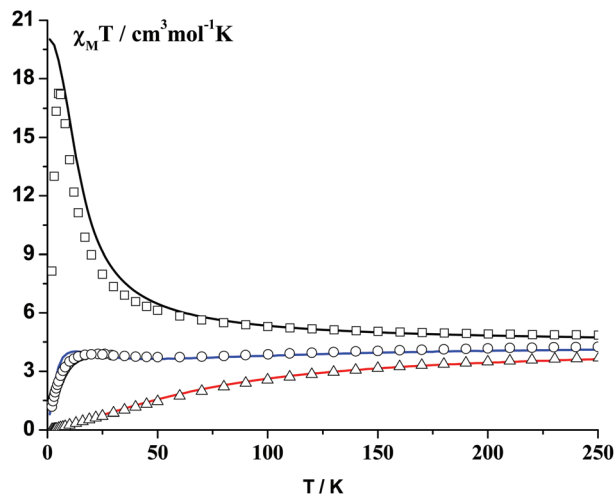


Fig. 7 $\chi_M T$ vs. T plot in the 300–2 K range of temperatures for **1** (squares), **2** (triangles) and **3** (circles). The $\chi_M T$ values obtained by means of quantum Monte Carlo simulations using the calculated DFT *J* values are plotted as continuous lines.

complexes, respectively. Thus, as most of the Cu(II) complexes have a Cu–N–Cu angle larger than 85° the tendency is in agreement with the “expected” behavior, larger Cu–N–Cu increases the antiferromagnetic contribution and the complexes become less ferromagnetic. For the Ni(II) complexes, the maximum strength of the ferromagnetic interaction appears for Ni–N–Ni angle values close to those adopted in most of the structures.⁴⁴ Thus, most of the Ni(II) azido bridging complexes show a small dispersion in the *J* values being ferromagnetic, and only a reported complex with a Ni–N–Ni angle value close to 90° presents antiferromagnetic behavior.⁴⁵ However, the Mn(II) complexes adopt Mn–N–Mn angle values smaller than that corresponding to the strongest ferromagnetic coupling. Thus, an increase of the Mn–N–Mn angle value enhances the ferromagnetism and such a tendency is just the opposite of the one usually assumed. This fact can be corroborated in Fig. 8 showing the dependence of the fitted *J* value for the reported EO azido Mn(II) complexes with the Mn–N–Mn angle value.

Table 5 Description of the bridging ligands, Mn...Mn and Mn–X distances (in Å) and bond angles (in degrees), and calculated exchange coupling constants *J* (cm^{−1}) for compounds **1–3**. The calculated values were obtained using the PBE functional with the SIESTA code (see the Computational methods section) and *J*_{fit} values are those extracted from the experimental measurements using a ring model

	Bridging ligands	Mn...Mn	Mn–N	Mn–N–Mn	<i>J</i> _{PBE}	<i>J</i> _{fit}
1						
<i>J</i> ₁	Two EO μ ₂ -N ₃	3.475	2.250–2.232–2.250–2.232	101.65	+2.4	+1.4
2						
<i>J</i> ₁	Two EO μ ₂ -N ₃	3.364	2.217–2.216–2.217–2.216	98.75	+0.12	+0.7
<i>J</i> ₂	Two EE μ ₂ -N ₃	5.030	2.240–2.245–2.245–2.240		−10.4	−12.8
3						
<i>J</i> ₁	Two EO μ ₂ -N ₃	3.474	2.248–2.248–2.242–2.242	101.38	+1.6	
<i>J</i> ₂	Two EO μ ₂ -N ₃	3.457	2.235–2.235–2.240–2.240	101.15	+1.6	
<i>J</i> ₃	Two EO μ ₂ -N ₃	5.141	2.239–2.239–2.243–2.243	101.39	+1.5	
<i>J</i> ₄	Two EO μ ₂ -N ₃	3.465	2.237–2.237–2.241–2.241	101.37	+1.3	
<i>J</i> ₅	Two EE μ ₂ -N ₃	5.141	2.221–2.221–2.220–2.220		−14.6	



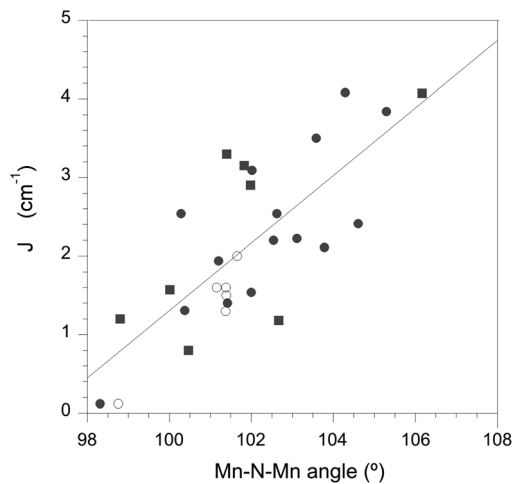


Fig. 8 Representation of the dependence of the reported experimental J values for dinuclear (black circles)^{43,46–54} and chain (black squares)^{10,55–60} azido-bridged Mn(II) compounds and those calculated in this work (white circles).

The calculated spin density of compound **1** is represented in Fig. 9. Surprisingly, the spin density of the bridging nitrogen atom of the azido groups shows negative spin density ($-0.07 e^-$) despite the fact that the d^5 configuration of the Mn(II) cations (spin population $4.8 e^-$). Such an electronic configuration implies the occupation of the “ e_g ” antibonding orbitals with a large mixing with the ligand orbitals; thus, it should be expected that such large orbital mixing will provide the same sign in the spin density of all the nitrogen atoms coordinated to the metal (spin delocalization mechanism) as happens with the pyrazine ligands (see Fig. 8).^{61,62} However, the opposite sign in such atoms indicates (also appears in compounds **2** and **3**) that the spin polarization mechanism is predominant; this result is different from that obtained either theoretically or experimentally for similar Cu(II) complexes.⁴²

In order to check if the opposite sign of the spin population of the bridging nitrogen atom is an artifact of the periodic PBE pseudopotential calculations, we performed all electron⁶³

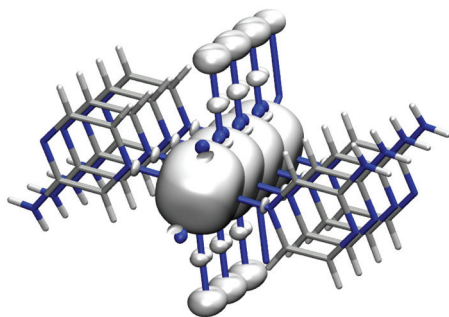


Fig. 9 Calculated spin density of compound **1**. White and blue isosurfaces indicate positive and negative spin populations, respectively, with a value of $0.003 e^- \text{ bohr}^{-3}$.

calculations of one Mn(II) end-on diazido dinuclear complex (FIBJIK, see Table S1†)⁴⁸ with the hybrid B3LYP functional⁶⁴ using the Gaussian code.⁶⁵ Again, such results confirm the negative spin population of the bridging nitrogen atoms ($-0.05 e^-$). The sign of the spin density in such nitrogen atoms is a subtle interplay between the spin delocalization of the singly-occupied antibonding e_g -type orbitals and the spin polarization caused by the singly-occupied t_{2g} -type orbitals. Usually, in such a case with singly-occupied antibonding e_g -type orbitals, the spin delocalization prevails over the spin polarization, as shown in Fig. 9 for the pyrazine ligands. However, the azido ligand has two π frontier orbitals (HOMO and LUMO) that very weakly interact with the in-phase and out-of-phase combinations of the two $d_{x^2-y^2}$ metal orbitals.⁶⁶ Thus, the two resulting molecular orbitals remain almost degenerate being consistent with the ferromagnetic character of the complexes with end-on azido bridging ligands. The weak interaction between the metal-azido orbitals results in a poor spin delocalization contribution (also reflected in the high spin population value of the Mn(II) centers around $4.8 e^-$) that is overcome by the spin polarization. To corroborate such assumptions, we repeated the DFT calculations for the dinuclear complex replacing the Mn(II) by Ni(II) cations (unpaired electrons in the two e_g -type orbitals, only spin delocalization) and V^{II} cations (unpaired electrons in the three t_{2g} -type orbitals, only spin polarization). In the case of the hypothetical dinuclear Ni(II) complex the spin population in the bridging nitrogen atom is only $+0.02 e^-$ while in the equivalent V^{II} system the value is $-0.07 e^-$ showing the predominance of the spin polarization. Finally, it is worth pointing out that the spin distribution found in the Mn(II) end-on diazido dinuclear complexes is similar to that proposed by Kahn and coworkers for Cu(II) end-on diazido dinuclear systems based on the so-called “spin polarization mechanism”⁶⁷ with opposite spin population in the bridging nitrogen atom while the terminal azido nitrogen atom has a relatively larger spin population with the same sign as the metal centers (see Fig. 8). This spin distribution was ruled out, either experimentally⁶⁸ or theoretically,⁴² for dinuclear Cu(II) systems but now we have found that it is present in the Mn(II) systems. Despite this fact the presence of ferromagnetic coupling in the family of end-on diazido dinuclear complexes is due to the accidental orthogonality of the orbitals bearing the unpaired electrons.⁶⁹

Conclusions

Here we have presented three new compounds with azido as the bridging ligand synthesized from the $S = 5/2$ Mn(II) cation and a terminal L ligand. The new compounds are: $[\text{Mn}(\text{N}_3)_2(\text{aminopyz})_2]_n$ (**1**), $[\text{Mn}(\text{N}_3)_2(4\text{-azpy})_2]_n$ (**2**) and $[\text{Mn}(\text{N}_3)_2(4\text{-Bzpy})_2]_n$ (**3**) (pyz = pyrazine (1,4-diazine), 4-azpy = 4-azido-pyridine and 4-Bzpy = 4-benzoylpyridine). The general formula is $[\text{Mn}(\text{N}_3)_2(\text{L})_2]_n$. Compounds **1–3** are representative of the great diversity of dimensionalities and topologies found in the Mn(II)-azido bridging compounds: **1** is a monodimensional



compound with double EO azido bridges, **2** is an alternating monodimensional compound with double end-on and double end-to-end azido bridges in the sequence di-EO-di-EE and **3** is a monodimensional compound with double end-on and double end-to-end azido bridges in the sequence di-EO-di-EO-diEO-di-EO-di-EE. Periodic calculations using PBE functionals to calculate the J values provide excellent agreement with the experimental data. The comparison was made by using quantum Monte Carlo simulations that allows the calculation of magnetic susceptibility curves for periodic systems. Also, it is worth noting that the theoretical analysis allows one to propose that in the range of experimental Mn–N–Mn bridging angle values, the calculated and observed trend is that larger angles result in stronger ferromagnetic coupling. Such a tendency is just the opposite of that usually expected, and is found in Cu(II) and Ni(II) complexes. The DFT spin density of the bridging nitrogen atoms of the azido ligands has the opposite sign of that of the Mn(II) centers. This result is not common because usually in the cases when the metal centers have unpaired electrons in the antibonding orbitals, the large metal–ligand mixing of orbitals results in that the spin delocalization effects are predominant over the spin polarization. In the studied end-on azido Mn(II) systems, the weak metal–ligand interaction is reflected in that the resulting molecular orbitals are close to the degeneracy, and that the spin polarization effects induced by the three singly-occupied “non-bonding” t_{2g} -type orbitals of the Mn(II) centers overcome the delocalization effect of the e_g -type orbitals. Logically, such “special” behavior cannot be found in Cu(II) or Ni(II) equivalent complexes because the t_{2g} -type orbitals are doubly-occupied.

Acknowledgements

R. V. acknowledges the financial support from the Spanish government grant CTQ2012-30662 and the Generalitat de Catalunya (Grant 2009SGR1454). E. R. acknowledges for an ICREA Academia grant (Generalitat de Catalunya) and for the grant CTQ2011-23862-C02-01 from the Spanish government. L. M. thanks Conicyt-Chile for a pre-doctoral fellowship. The computer resources, technical expertise and assistance provided by the Barcelona Supercomputing Centre are also acknowledged.

References

- J. Ribas, A. Escuer, M. Monfort, R. Vicente, R. Cortés, L. Lezama and T. Rojo, *Coord. Chem. Rev.*, 1999, **193–195**, 1027.
- B. Bitschnau, A. Egger, A. Escuer, F.A. Mautner, B. Sodin and R. Vicente, *Inorg. Chem.*, 2006, **45**, 868, and references therein.
- X.-Y. Wang, B.-L. Li, X. Zhu and S. Gao, *Eur. J. Inorg. Chem.*, 2005, 3277.
- M.A.M. Abu-Youssef, A. Escuer and V. Langer, *Eur. J. Inorg. Chem.*, 2005, 4659.
- W. Zhao, Y. Song, T.-A. Okamura, J. Fan, W.-Y. Sun and N. Ueyama, *Inorg. Chem.*, 2005, **44**, 3330.
- E.-Q. Gao, A.-L. Cheng, Y.-X. Xu, M.-Y. He and C.-H. Yan, *Inorg. Chem.*, 2005, **44**, 8822.
- H.-R. Wen, C.-F. Wang, Y. Song, J.-L. Zuo and X.-Z. You, *Inorg. Chem.*, 2005, **44**, 9039.
- M. A. M. Abu-Youssef, A. Escuer and V. Langer, *Eur. J. Inorg. Chem.*, 2006, 3177.
- S.Q. Bai, E. Q. Gao, Z. He, C.-J. Fang, Y.-F. Yue and C.-H. Yan, *Eur. J. Inorg. Chem.*, 2006, 407.
- A. Das, G. M. Rosair, M. Salah El Fallah, J. Ribas and S. Mitra, *Inorg. Chem.*, 2006, **45**, 3301.
- P. Bhuina, V. S. Ray, G. Mostafa, J. Ribas and C. Sinha, *Inorg. Chim. Acta*, 2006, **359**, 4660.
- F.-C. Liu, Y.-F. Zeng, J.-P. Zhao, B.-W. Hu, X.-H. Bu, J. Ribas and J. Cano, *Inorg. Chem.*, 2007, **46**, 1520.
- J.-Y. Zhang, C.-M. Liu, D.-Q. Zhang, S. Gao and D.-B. Zhu, *Inorg. Chem. Commun.*, 2007, **10**, 897.
- M.A.M. Abu-Youssef, A. Escuer, M. A. S. Goher, F. A. Mautner, G. J. Reiss and R. Vicente, *Angew. Chem., Int. Ed.*, 2000, **39**, 1624.
- (a) A. Escuer, F. A. Mautner, M. A. S. Goher, M.A. M. Abu-Youssef and R. Vicente, *Chem. Commun.*, 2005, 605; (b) F.A. Mautner, A. Egger, B. Sodin, M.A.S. Goher, M.A.M. Abu-Youssef, A. Massoud, A. Escuer and R. Vicente, *J. Mol. Struct.*, 2010, **969**, 192.
- (a) T.A. Richter, *Energetic Materials*, ed. H.D. Fair and R.F. Walker, Plenum Press, New York, 1977, vol. I, pp. 25–31; (b) R. Vicente, B. Bitschnau, A. Egger, B. Sodin and F.A. Mautner, *Dalton Trans.*, 2009, 5120.
- G. Labbe and L. Beenaerts, *Tetrahedron*, 1989, **45**, 749.
- SADABS Bruker AXS, *Software Reference Manual*, Madison, WI, 1998.
- G.M. Sheldrick, *Acta Crystallogr., Sect. A: Found. Crystallogr.*, 2008, **64**, 112.
- C.F. Macrae, P.R. Edington, P. McCabe, E. Pidcock, G.P. Shields, R. Taylor, T. Towler and J. van de Streek, *J. Appl. Crystallogr.*, 2006, **39**, 453.
- E. Artacho, J.M. Cela, J.D. Gale, A. García, J. Junquera, R.M. Martin, P. Ordejón, D. Sánchez-Portal and J.M. Soler, *Siesta 3.0*, 2010.
- E. Artacho, D. Sánchez-Portal, P. Ordejón, A. García and J.M. Soler, *Phys. Status Solidi A*, 1999, **215**, 809.
- J.M. Soler, E. Artacho, J.D. Gale, A. García, J. Junquera, P. Ordejón and D. Sánchez-Portal, *J. Phys.: Condens. Matter*, 2002, **14**, 2745.
- J. Perdew, K. Burke and M. Ernzerhof, *Phys. Rev. Lett.*, 1996, **77**, 3865.
- V.I. Anisimov, F. Aryasetiawan and A.I. Lichtenstein, *J. Phys.: Condens. Matter*, 1997, **9**, 767.
- L. Kleinman and D.M. Bylander, *Phys. Rev. Lett.*, 1982, **48**, 1425.
- N. Trouiller and J.L. Martins, *Phys. Rev. B: Condens. Matter*, 1991, **43**, 1993.
- E. Ruiz, T. Cauchy, J. Cano, R. Costa, J. Tercero and S. Alvarez, *J. Am. Chem. Soc.*, 2008, **130**, 7420.



- 29 E. Ruiz, A. Rodríguez-Forteza, J. Tercero, T. Cauchy and C. Massobrio, *J. Chem. Phys.*, 2005, **123**, 074102.
- 30 E. Ruiz, P. Alemany, S. Alvarez and J. Cano, *J. Am. Chem. Soc.*, 1997, **119**, 1297.
- 31 E. Ruiz, S. Alvarez, J. Cano and V. Polo, *J. Chem. Phys.*, 2005, **123**, 164110.
- 32 E. Ruiz, *Struct. Bonding*, 2004, **113**, 71.
- 33 E. Ruiz, A. Rodríguez-Forteza, J. Cano, S. Alvarez and P. Alemany, *J. Comput. Chem.*, 2003, **24**, 982.
- 34 E. Ruiz, M. Llunell and P. Alemany, *J. Solid State Chem.*, 2003, **176**, 400.
- 35 A.W. Sandvik, *Phys. Rev. B: Condens. Matter*, 1999, **59**, 14157.
- 36 A.F. Albuquerque, F. Alet, P. Corboz, P. Dayal, A. Feiguin, S. Fuchs, L. Gamper, E. Gull, S. Gürtler, A. Honecker, R. Igarashi, M. Körner, A. Kozhevnikov, A. Läuchli, S.R. Manmana, M. Matsumoto, I.P. McCulloch, F. Michel, R.M. Noack, G. Pawłowski, L. Pollet, T. Pruschke, U. Schollwöck, S. Todo, S. Trebst, M. Troyer, P. Werner and S. Wessel, *J. Magn. Magn. Mater.*, 2007, **310**, 1187.
- 37 B. Bauer, L.D. Carr, H.G. Evertz, A. Feiguin, J. Freire, S. Fuchs, L. Gamper, J. Gukelberger, E. Gull, S. Guertler, A. Hehn, R. Igarashi, S.V. Isakov, D. Koop, P.N. Ma, P. Mates, H. Matsuo, O. Parcollet, G. Pawłowski, J.D. Picon, L. Pollet, E. Santos, V.W. Scarola, U. Schollwöck, C. Silva, B. Surer, S. Todo, S. Trebst, M. Troyer, M.L. Wall, P. Werner and S. Wessel, *J. Stat. Mech.: Theory Exp.*, 2011, **2011**, P05001.
- 38 M. E. Fisher, *Am. J. Physiol.*, 1964, **32**, 343.
- 39 M.A.M. Abu-Youssef, A. Escuer, D. Gatteschi, M. A. S. Goher, F. Mautner and R. Vicente, *Inorg. Chem.*, 1999, **38**, 5716.
- 40 M.A.M. Abu-Youssef, A. Escuer and V. Langer, *Eur. J. Inorg. Chem.*, 2006, 3177.
- 41 R. Cortés, M. Drillon, X. Solans, L. Lezama and T. Rojo, *Inorg. Chem.*, 1997, **36**, 677.
- 42 E. Ruiz, J. Cano, S. Alvarez and P. Alemany, *J. Am. Chem. Soc.*, 1998, **120**, 11122.
- 43 T.K. Karmakar, B.K. Ghosh, A. Usman, H.-K. Fun, E. Rivière, T. Mallah, G. Aromí and S.K. Chandra, *Inorg. Chem.*, 2005, **44**, 2391.
- 44 G. Manca, J. Cano and E. Ruiz, *Inorg. Chem.*, 2009, **48**, 3139.
- 45 P. Chaudhuri, R. Wagner, S. Khanra and T. Weyhermuller, *Dalton Trans.*, 2006, 4962.
- 46 H. Hosseini-Monfared, R. Bikas, J. Sanchiz, T. Lis, M. Siczek, J. Tucek, R. Zboril and P. Mayer, *Polyhedron*, 2013, **61**, 45.
- 47 H.-P. Jia, W. Li, Z.-F. Ju and J. Zhang, *Inorg. Chem. Commun.*, 2007, **10**, 397.
- 48 C.-M. Liu, S. Gao, D.-Q. Zhang, Z.-L. Liu and D.-B. Zhu, *Inorg. Chim. Acta*, 2005, **358**, 834.
- 49 R. Cortes, J.L. Pizarro, L. Lezama, M.I. Arriortua and T. Rojo, *Inorg. Chem.*, 1994, **33**, 2697.
- 50 H.-Y. Wu, H.-Q. An, B.-L. Zhu, S.-R. Wang, S.-M. Zhang, S.-H. Wu and W.-P. Huang, *Inorg. Chem. Commun.*, 2007, **10**, 1132.
- 51 M.-M. Yu, Z.-H. Ni, C.-C. Zhao, A.-L. Cui and H.-Z. Kou, *Eur. J. Inorg. Chem.*, 2007, 5670.
- 52 Z.-S. Meng, L. Yun, W.-X. Zhang, C.-G. Hong, R. Herchel, Y.-C. Ou, J.-D. Leng, M.-X. Peng, Z.-J. Lin and M.-L. Tong, *Dalton Trans.*, 2009, 10284.
- 53 Z.-H. Ni, H.-Z. Kou, L. Zheng, Y.-H. Zhao, L.-F. Zhang, R.-J. Wang, A.-L. Cui and O. Sato, *Inorg. Chem.*, 2005, **44**, 4728.
- 54 C.-H. Ge, A.-L. Cui, Z.-H. Ni, Y.-B. Jiang, L.-F. Zhang, J. Ribas and H.-Z. Kou, *Inorg. Chem.*, 2006, **45**, 4883.
- 55 Y.-Q. Wang, Q.-X. Jia, K. Wang, A.-L. Cheng and E.-Q. Gao, *Inorg. Chem.*, 2010, **49**, 1551.
- 56 M.A.M. Abu-Youssef, A. Escuer, M.A.S. Goher, F.A. Mautner and R. Vicente, *J. Chem. Soc., Dalton Trans.*, 2000, 413.
- 57 T.K. Karmakar, G. Aromi, B.K. Ghosh, A. Usman, H.-K. Fun, T. Mallah, U. Behrens, X. Solans and S.K. Chandra, *J. Mater. Chem.*, 2006, **16**, 278.
- 58 Y.-Q. Wang, Q. Sun, Q. Yue, A.-L. Cheng, Y. Song and E.-Q. Gao, *Dalton Trans.*, 2011, **40**, 10966.
- 59 A. Das, G.M. Rosair, M.S. El Fallah, J. Ribas and S. Mitra, *Inorg. Chem.*, 2006, **45**, 3301.
- 60 J.L. Manson, A.M. Arif and J.S. Miller, *Chem. Commun.*, 1999, 1479.
- 61 J. Cano, E. Ruiz, S. Alvarez and M. Verdaguier, *Comments Inorg. Chem.*, 1998, **20**, 27.
- 62 E. Ruiz, J. Cirera and S. Alvarez, *Coord. Chem. Rev.*, 2005, **249**, 2649.
- 63 A. Schaefer, C. Huber and R. Ahlrichs, *J. Chem. Phys.*, 1994, **100**, 5829.
- 64 A.D. Becke, *J. Chem. Phys.*, 1993, **98**, 5648.
- 65 M. J. Frisch, G.W. Trucks, H.B. Schlegel, G.E. Scuseria, M.A. Robb, J.R. Cheeseman, G. Scalmani, V. Barone, B. Mennucci, G.A. Petersson, H. Nakatsuji, M. Caricato, X. Li, H.P. Hratchian, A.F. Zmaylov, I.J. Bloino, G. Zheng, J.L. Sonnenberg, M. Hada, M. Ehara, K. Toyota, R. Fukuda, J. Hasegawa, M. Ishida, T. Nakajima, Y. Honda, O. Kitao, H. Nakai, T. Vreven, J.J.A. Montgomery, J.E. Peralta, F. Ogliaro, M. Bearpark, J.J. Heyd, E. Brothers, K.N. Kudin, V.N. Staroverov, R. Kobayashi, J. Normand, K. Raghavachari, A. Rendell, J.C. Burant, S.S. Iyengar, J. Tomasi, M. Cossi, N. Rega, J.M. Millam, M. Klene, J.E. Knox, J.B. Cross, V. Bakken, C. Adamo, J. Jaramillo, R. Gomperts, R.E. Stratmann, O. Yazyev, A.J. Austin, C. Cammi, J.W. Pomelli, R. Ochterski, R.L. Martin, K. Morokuma, V.G. Zakrzewski, G.A. Voth, P. Salvador, J.J. Dannenberg, S. Dapprich, A.D. Daniels, O. Farkas, J.B. Foresman, J.V. Ortiz, J. Cioslowski and D.J. Fox, *Gaussian 09 (Revision D01)*, C.T. Wallingford, 2009.
- 66 I. Seggern, F. Tucek and W. Bensch, *Inorg. Chem.*, 1995, **34**, 5530.
- 67 M.-F. Charlot, O. Kahn, M. Chaillet and C. Larrieu, *J. Am. Chem. Soc.*, 1986, **108**, 2574.
- 68 M.A. Aebersold, M. Gillon, O. Plantevin, L. Pardi, O. Kahn, P. Bergerat, I.F.T. von Seggern, L. Ohrström, A. Grand and E. Lelièvre-Berna, *J. Am. Chem. Soc.*, 1998, **120**, 5238.
- 69 R. Vicente, A. Escuer, J. Ribas, M.S. El Fallah, X. Solans and M. Font-Bardia, *Inorg. Chem.*, 1993, **32**, 1920.

